Astron. Astrophys. 326, 537–553 (1997)

ASTRONOMY
AND
ASTROPHYSICS

Gas segregation in the interacting system Arp 105

P.–A. Duc[1,2], **E. Brinks**[3,4], **J.E. Wink**[5], **and I.F. Mirabel**[2]

[1] ESO, Karl–Schwarzschild–Str. 2, D-85748 Garching bei München, Germany
[2] CEA, DSM, DAPNIA, Service d'Astrophysique, C.E. Saclay, F-91191 Gif sur Yvette Cedex, France
[3] NRAO, P.O. Box O, Socorro, NM 87801–0387, USA
[4] Departamento de Astronomía, Universidad de Guanajuato, Apdo. Postal 144, Guanajuato, C.P. 36000, México
[5] IRAM, 300, rue de la Piscine, F-38406 Saint–Martin–d'Hères Cedex, France

Received 27 January 1997 / Accepted 30 April 1997

Abstract. Arp 105 is an example of a collision between an infrared luminous spiral (NGC 3561A) and an elliptical (NGC 3561B) galaxy in a cluster of galaxies. Duc & Mirabel (1994) reported in this system the genesis of star–forming tidal dwarf galaxies at the ends of the tidal tails emanating from the spiral. In this paper, the gas distribution in Arp 105 is analyzed based on HI and ^{12}CO(1–0) emission, mapped with the Very Large Array and the Plateau de Bure interferometers. The observations reveal an extreme segregation between the atomic and molecular gas distributions. HI clouds as massive as 6×10^9 $M_\odot$ are found along the tidal tails and are associated with the dwarf galaxies at their tip; the spiral disk itself contains less than 5×10^7 $M_\odot$ of HI. About 10^{10} $M_\odot$ of molecular gas is concentrated in the central 3 kpc region of the spiral. Towards the elliptical, HI is seen in absorption. The shape of the absorption line suggests inflow and capture of gas by the giant galaxy. Arp 105 thus shows direct evidence of mass transfer between a spiral and an elliptical. All these phenomena are interpretated as a direct consequence of the interaction between NGC 3561A and B. A study of the dynamics of the system reveal that the HI in the northern tail is composed of two individual components, one along the optical tail, and a second one, kinematically decoupled, which shows signs of rotation. Indications of rotation are also seen in H_α in the tidal object at the tip of the southern tail. These observations show that these tidal dwarf galaxies might have already acquired dynamical independence.

Key words: galaxies–individual: Arp 105 – galaxies: interactions – galaxies: formation – galaxies: ISM – galaxies: kinematics and dynamics – radio lines: galaxies

1. Introduction

Collisions cause major perturbations in the stellar and gaseous contents of galaxies. The optical disks of spirals may be torn into elongated structures to form the tails, bridges, and shells which feature prominently in catalogues of interacting galaxies (Vorontsov-Velyaminov, 1959; Arp, 1966; Arp & Madore, 1987); in addition, the distribution of the different gas components becomes highly perturbed. Whereas unusually high concentrations of molecular gas have been detected in the core of mergers (Sargent & Scoville, 1991; Scoville et al., 1991), HI gas clouds are found in the outskirts of interacting systems, along and mostly at the end of optical tails emanating from the colliding bodies (van der Hulst, 1979; Hibbard, 1995). All these phenomena may be explained by gravitational disturbances, although some other environmental effects, like ram pressure by intracluster gas (Gunn & Gott, 1972), cannot be excluded. Numerical simulations (Toomre & Toomre, 1972; Barnes & Hernquist, 1992; Elmegreen et al., 1993; Hibbard & Mihos, 1995) have played a crucial role in demonstrating how tidal forces shape the stellar and gaseous structures in interacting systems. Moreover, interactions are capable of triggering star formation. Vigorous starbursts are found associated with the molecular clumps in the central regions (Sargent & Scoville, 1991), whereas material pulled into extragalactic space may form new objects known as tidal dwarf galaxies (Schweizer, 1978; Mirabel et al., 1992; Duc, 1995).

One of the clearest objects where both these phenomena can be observed is the interacting system Arp 105, studied in detail in Duc & Mirabel (1994) (hereafter Paper I). Arp 105, which is situated at a distance of 115 Mpc[1], is an example of a close encounter between a gas rich spiral, NGC 3561A, and an elliptical galaxy, NGC 3561B, near the centre of the galaxy cluster Abell 1185. Some general properties of both galaxies are summarized in Table 1. Two tidal tails emanate from NGC 3561A. The northern, 100 kpc long tail, hosts at its tip an irregular galaxy of Magellanic type, hereafter referred to as A105N. The

Send offprint requests to: pduc@eso.org

[1] In this paper, we use H_0 = 75 km s^{-1} Mpc^{-1}

Table 1. Arp 105: miscellaneous data

NGC 3561A: Optical Position	$\alpha_{B1950} = 11^h08^m31\overset{s}{.}33$
	$\delta_{B1950} = 28°58'59\overset{''}{.}9$
NGC 3561A: 6 cm Position [+]	$\alpha_{B1950} = 11^h08^m31\overset{s}{.}3$
	$\delta_{B1950} = 28°58'59''$
Adopted Distance[*]	D = 115 Mpc
	$1'' \sim 0.6$ kpc
NGC 3561A: Absolute Magnitude	$M_B = -19.8$
NGC 3561B: Absolute Magnitude	$M_B = -20.3$

[*] H_0 = 75 km s^{-1} Mpc^{-1}
[+]Batuski et al. (1992), from VLA-B observations

Table 2. VLA Observing Parameters

Configuration	D	C
Dates	Nov 1993	Oct 1994
Velocity Center (km s^{-1})	8775	8775
Time on Source (hrs)	4.0	13.0
Configuration	C+D	
Synthesized Beam	$23\overset{''}{.}3 \times 21\overset{''}{.}0$	
Beam Position Angle	-45 °	
Conversion to T_B	1 mJy beam^{-1} = 1.23 K	
Velocity Range	8400–9000 km s^{-1}	
Number of Channels	64	
Channel Separation	10.9 km s^{-1}	
Noise level per channel (1 σ)	0.33 mJy beam^{-1}	

southern filament, which appears at its base as a weak, diffuse counter–tail, crosses the elliptical and ends in a blue compact dwarf galaxy, referred to as A105S. North of the latter object, the tail also hosts several compact HII regions. The two small galaxies A105S and A105N contain active star–forming regions. In Paper I, we have reported on optical photometry and spectroscopy, as well as single dish HI and CO observations of this system.

In this article, detailed maps of the HI and CO gas distributions, derived from interferometric radio data, are presented. The observations were carried out with the NRAO[2]–Very Large Array (VLA) in two configurations to map the HI 21–cm line and with the IRAM Plateau de Bure (PdB) interferometer to measure the distribution of the ^{12}CO(1–0) emission.

2. Observations

2.1. VLA HI observations

The HI observations were made in two configurations. We used the VLA D–configuration (maximum baseline 1.03 km) on 8 November 1993 to observe the Arp 105 field. Two sessions in C–configuration (maximum baseline 3.4 km) were added, on 20 and 27 October 1994. The observational set–up is listed in Table 2. For a description of the VLA, see the article by Napier et al. (1983). As always, one has to trade off spectral resolution against velocity coverage. Our aim was to get 10 km s^{-1} after Hanning smoothing the data, which normally is obtained by calculating a 64 channel spectrum over 3.125 MHz, corresponding to a velocity range of about 600 km s^{-1}, and recording the signal in both right hand (R) as well as left hand (L) polarizations. Because the sensitivity drops off rapidly at the edges of the band, this set–up effectively covers a velocity range of 450 km s^{-1}. As we were not entirely sure about the range over which we could expect HI emission, and 450 km s^{-1} would not have been sufficient to record line–free channels which are to be used to subtract the continuum emission, we decided to err on the safe side and use the capability of the VLA to tune the R and L polarizations to different frequencies (or central velocities). The band receiving R signal was centred at 8775 km s^{-1}, the one recording L signal was at about 8622 km s^{-1}. Thus, after deleting those channels which are near the edge of the passband, we covered the velocity range from 8400 km s^{-1} to 9000 km s^{-1}; full sensitivity was obtained from about 8550 to 8850 km s^{-1}, the remaining channels being less sensitive by a factor of $\sqrt{2}$ as only one polarization is available (either R or L).

We used source 1328+307 (3C286) for absolute flux calibration and to determine the bandpass. We assumed a flux density of 15.06 Jy on the scale. Our secondary calibrator was 1153+317 which was observed on average every 30 minutes for 3 minutes. Its flux density was measured to be 3.05 Jy. The data were calibrated and mapped using the NRAO AIPS package.

Solar interference was visible in the D–array observations. As the data were taken before and after sunrise, part of the data were unaffected. As solar interference is concentrated on the shorter wavelengths, and as the *uv*–plane substantially oversamples these shorter spacings, we decided to edit out the shorter spacings (shortward of 2.3 kλ) which were recorded after sunrise (or about $2/3$ of the run). This hardly increased the noise level in the maps and virtually eliminated the effects of the Sun.

The three sets of observations were merged in *uv*–space and Fourier transformed to yield maps of the HI distribution. A data cube was produced, using natural weighting, which has the lowest noise of 0.21 mJy beam^{-1} channel^{-1} at an angular resolution of $23.3'' \times 21.0''$ (note that the noise value is for those channels where both R and L polarizations were measured). The data were blanked at the 2.5σ level and those features which were present in at least 3 consecutive channel maps were retained. Out of 64 useful channels (after merging the overlapping bands), channels 12 until 47 contain line emission. Except for channel 12, all these channels have both R and L polarization data. The remaining channels provided the continuum which was subtracted in the map plane. The continuum subtracted maps were cleaned down to a level of 0.5 mJy beam^{-1}. Moment maps were calculated based on the blanked data.

2.2. ^{12}CO(1–0) PdB observations

The CO observations were centred on the redshifted restfrequency of 112.0022 GHz and were carried out between January

[2] The NRAO is a facility of the the National Science Foundation, operated under cooperative agreement by Associated Universities, Inc.

Table 3. Plateau de Bure Observing Parameters

Frequency	112.0022 GHz
Dates	January – March 1994
Configuration	BC (4 antennae)
Synthesized Beam	$2\farcs8\times2\farcs0$
Beam Position Angle	+53 °
Conversion to T_B	1 mJy beam^{-1}= 0.018 K
Velocity Range	8400–9100 km s^{-1}
Number of Channels	101
Channel Separation	6.7 km s^{-1}
Noise level (10 km s^{-1})	7.2 mJy beam^{-1}

and March 1994 with the IRAM 4 element interferometer under excellent weather conditions. We divided our time between two pointings, one towards the spiral and one towards the elliptical. A detailed description of this instrument was presented by Guilloteau et al. (1992). Table 3 summarizes the observing parameters. We used 5 configurations with baselines extending out to 280 m (BC configuration set). The observing sequence consisted of 4 min integrations on the calibrator 1156+295 followed by 16 min on the spiral and 4 min on the elliptical galaxy. Typical SSB system temperatures were 350 K. We configured the 6 correlator units to give 0.625 MHz channel spacing for the inner 220 MHz wide band and 2.5 MHz spacing for the inner 400 MHz band. The bands were overlapping to avoid the Gibbs phenomenon and edge effects. Amplitude and phase calibration was done against 1156+295, which itself was referred against 0316+413 (3C84), 0923+392, 1226+023 (3C273), and 1749+096, at least one of which was observed each day to calibrate the bandpass of the receiver. During the 3 observing months we noted no flux variation for 1156+295 at a limit of 20% and used a flux of 1.7 Jy for amplitude calibration.

The data were calibrated and analyzed with the CLIC and GRAPHIC software packages developed at IRAM and Observatoire de Grenoble. For the spectral maps original channels were combined to achieve a 10 MHz spacing or 6.7 km s^{-1} velocity resolution. Map sizes were 128 x 128 cells of $0.5''\times0.5''$ each. The synthesized beams were $2.8''\times2.0''$ at position angle 53° (1.7 kpc $\times$1.2 kpc) for both spiral and elliptical field centres. The conversion from flux density into main beam brightness temperature was calculated assuming the Rayleigh-Jeans approximation.

2.3. Astrometry

In order to superimpose the gas distributions on the optical image of the system, careful astrometry of the field had to be performed. This is particularly critical when making comparisons between CO and the optical because of their relatively high spatial resolution. The astrometric errors at 112 GHz are less than $0\farcs2$. The optical image used in this paper was taken during an observing run carried out in January 1992 at the Canada–France–Hawaii Telescope (Paper I). The pixel size was $0\farcs34$ and the seeing $0\farcs8$. Unfortunately only 4 Guide Star Catalog objects, all extended, and no Proper Motion Stars were present in the $5\farcm8$ x $5\farcm8$ field of the CFHT image. In order to obtain an astrometric solution, corrected for distortion, secondary reference sources had to be used. These were found in a STScI Digital Sky Survey field, the astrometry of which had previously been determined on a larger field of $20'$ x $20'$, using 34 GSC sources. The positions of 11 secondary stars were determined that way. A 3rd degree 2D polynomial transformation was applied to the original frame, using IRAF. The relative astrometric precision obtained that way was better than $0\farcs7$. The absolute astrometry was afterwards derived from the position of a QSO (QS1108+285) present in our field, the coordinates of which had been determined by Veron et al. (1976), with a precision of $0\farcs5$.

3. Results

Fig. 1 shows the HI (in green) and CO(1–0) (in black) integrated column density distributions, superimposed on an optical V band image obtained at the CFHT. The most striking result is the marked spatial separation between the atomic hydrogen gas and the molecular gas as traced by the CO emission. Almost no HI is detected towards the spiral whereas this galaxy contains high quantities of molecular gas. HI emission is predominantly seen along the northern tidal tail, and to a smaller extent along the southern filament. In what follows, we will discuss the gas distributions in more detail.

3.1. The HI gas

The observational results of our HI observations are presented in the following figures: in addtion to Fig. 1, Fig. 2 displays the individual profiles of the 21 cm line in the southern part of the system; Fig. 3 shows the individual channel maps of the 21 cm line, separated by intervals of 20 km s^{-1}, superimposed on the optical V–Band image; and Fig. 6 presents the HI velocity map. Table 4 summarizes the HI integrated properties of the system: the angular and linear sizes of the HI clouds (Col. 2,3), the peak column density (Col. 4), the HI masses (Col. 5), derived using the formula by Giovanelli & Haynes (1988), and the FWHM of the 21 cm line (Col. 6), integrated over the entire cloud extent.

3.1.1. The spiral galaxy

No HI is found coinciding with the spiral galaxy itself, except perhaps for a small cloud of mass 5×10^7M$_\odot$, at the detection limit of the VLA. It is located to the NW of the disk next to a star forming region.

3.1.2. The northern tail (Cloud A105N)

As shown in Fig. 1, the bulk of the atomic hydrogen is distributed along the northern optical tidal tail. The peak of emission is situated on the Magellanic irregular galaxy (A105N), and more precisely at a distance of 110 kpc from the nucleus of NGC 3561A. It coincides with optical knots which were found

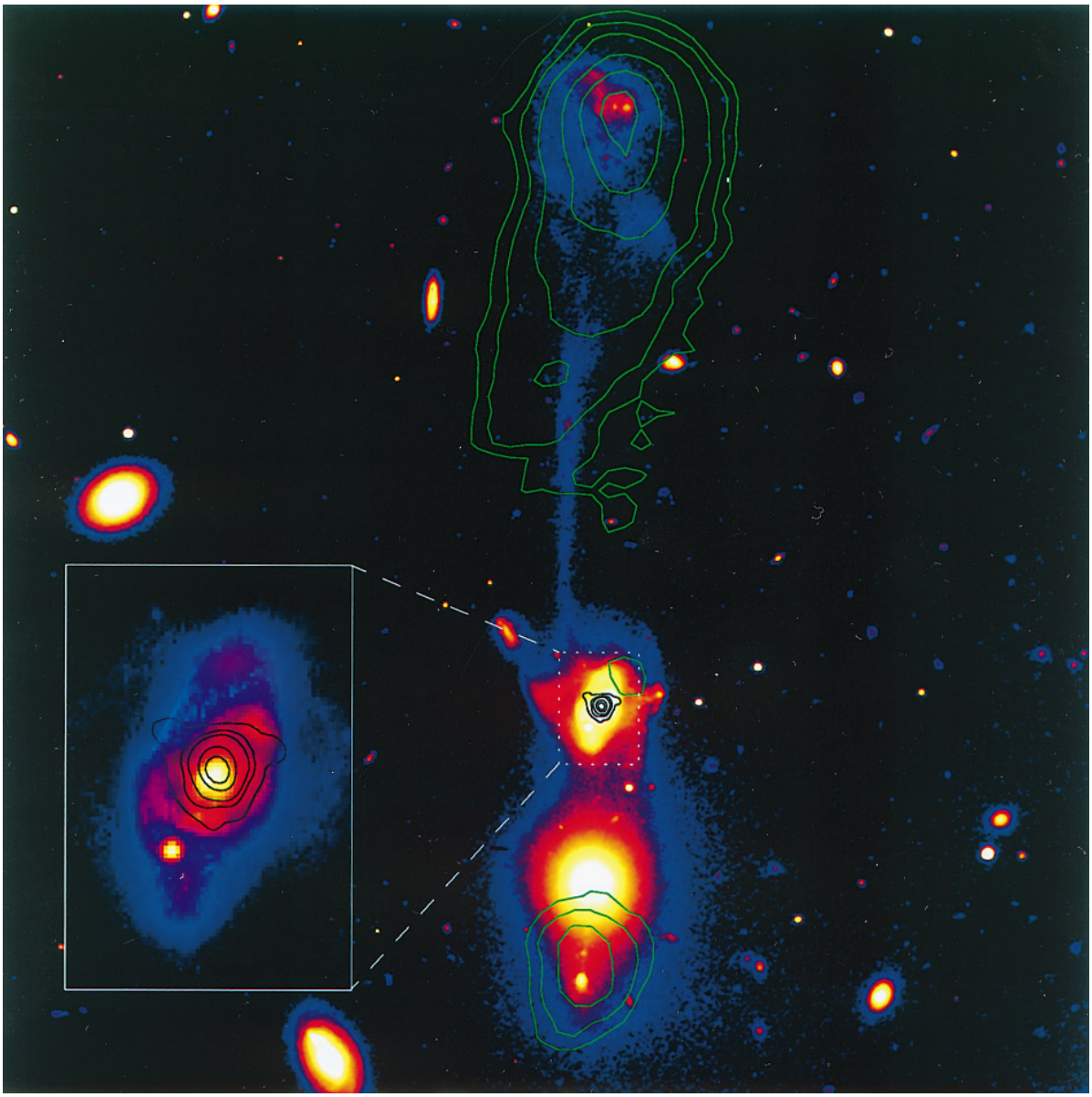

Fig. 1. Gas segregation in Arp 105, a starburst spiral galaxy, torn apart by an elliptical in a cluster of galaxies. Superimposed on a V band CFHT image is shown the HI mapped with the Very Large Array (green contours), which peaks at the position of star–forming dwarf galaxies located at the ends of tidal tails. The molecular gas traced by the CO observations (black contours) with the Plateau de Bure interferometer is concentrated in a 3 kpc radius region of the infrared luminous spiral. The field of view is $5'.8 \times 5'.8$ (200 kpc $\times$200 kpc, H_0 = 75 km s^{-1} Mpc^{-1}). The VLA and PdB beam sizes were resp. $23''.3 \times 21''.0$ (PA=-45°) and $2''.8 \times 2''.0$ (PA=+52°). North is up and East left. The HI contour levels are 0.5, 1.1, 2.2, 4.5, 6.7, 8.9 $\times 10^{20}$ cm^{-2}. The CO contour levels are 2.0, 4.7, 6.7, 13.4, 10.0 Jy km s^{-1}.beam^{-1}

to be HII regions (Paper I). This cloud will be referred hereafter as Cloud A105N. The HI distribution is highly asymmetric. Getting closer to the spiral, the HI column density gradually decreases, dropping below 5×10^{19} cm^{-2} at a distance of 30 kpc from the nucleus of the spiral. The total HI mass of Cloud A105N, 6.6×10^9 M$_\odot$, is slightly higher than that determined from single dish Arecibo observations (6.0×10^9 M$_\odot$, Paper I). Fig. 3 reveals unexpected and complicated features in the HI kinematics. In A105N, several components at different velocities coexist along the line of sight. This explains, in particular, the unusually high HI velocity dispersion in Cloud A105N — it has a mean value of 25 km s^{-1} and peaks at 70 km s^{-1} in the diffuse feature, west of the Magellanic Irregular —, and makes the determination of a single mean velocity from the peak of the HI emission line (Fig. 6) rather ambiguous. Nevertheless, the velocity determined towards the HII regions in A105N matches that measured in the optical (see Table 7). We will look into the detailed kinematics of this arm in Sect 4.2.1.

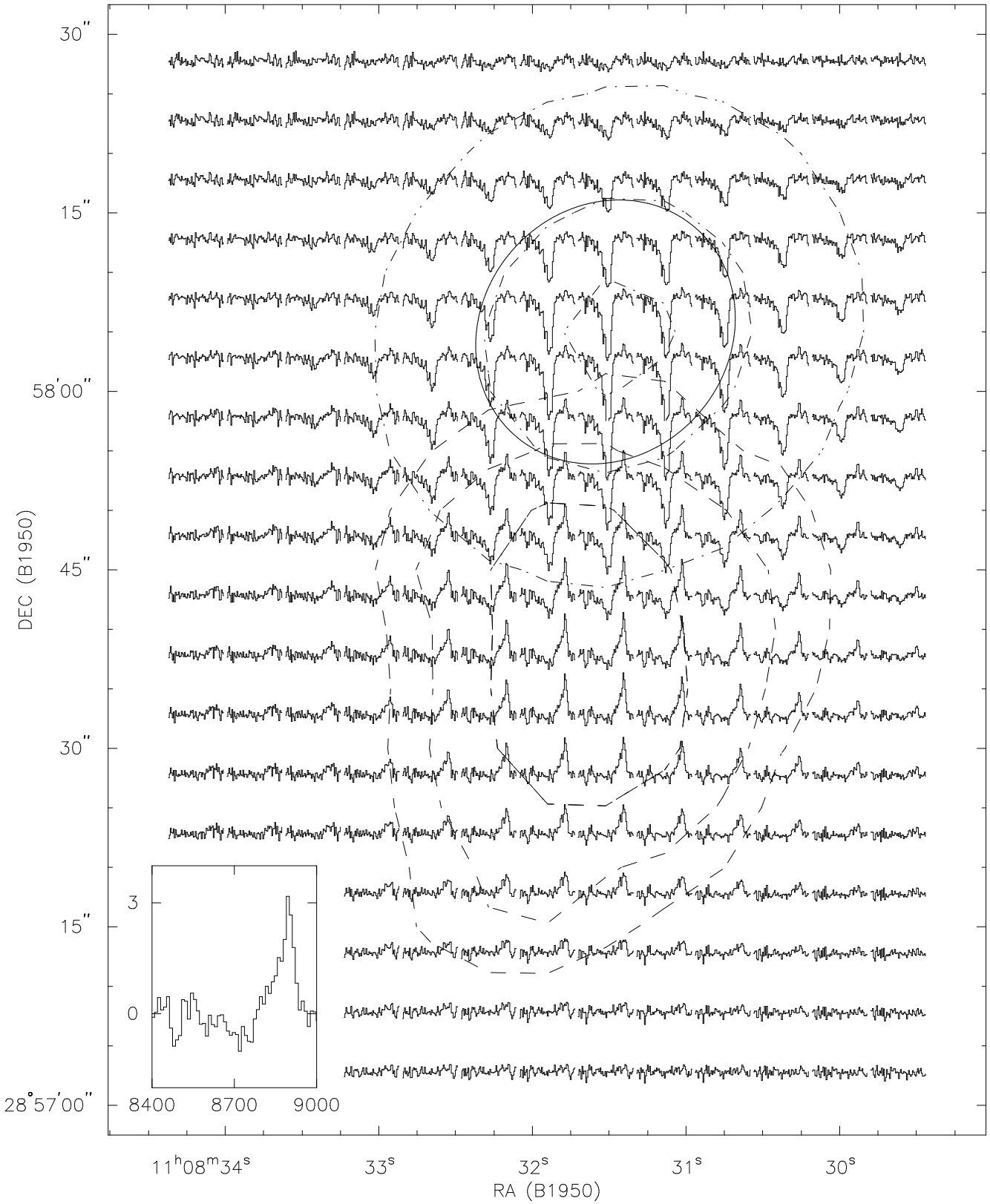

Fig. 2. Individual HI spectra of the southern region of Arp 105, encompassing NGC 3561B and A105S. Whereas HI in emission is found along the southern tail, an HI absorption cloud is seen in front of the elliptical galaxy, known to be a compact radiosource. Each spectrum corresponds to an area of $5'' \times 5''$. A closeup of the HI line corresponding to the emission peak, with the scale units (km s^{-1}, mJy $beam^{-1}$), is shown in the lower left hand corner. The contours of the integrated column density are superimposed (dashed lines). Also shown the contours of the continuum 20 cm emission of NGC 3561B (dot–dashed lines). Levels correspond to 90%, 50% and 10% of the peak flux (42.4 mJy). Comparing it with the VLA beam size (plain ellipse), one sees that the radiosource is unresolved

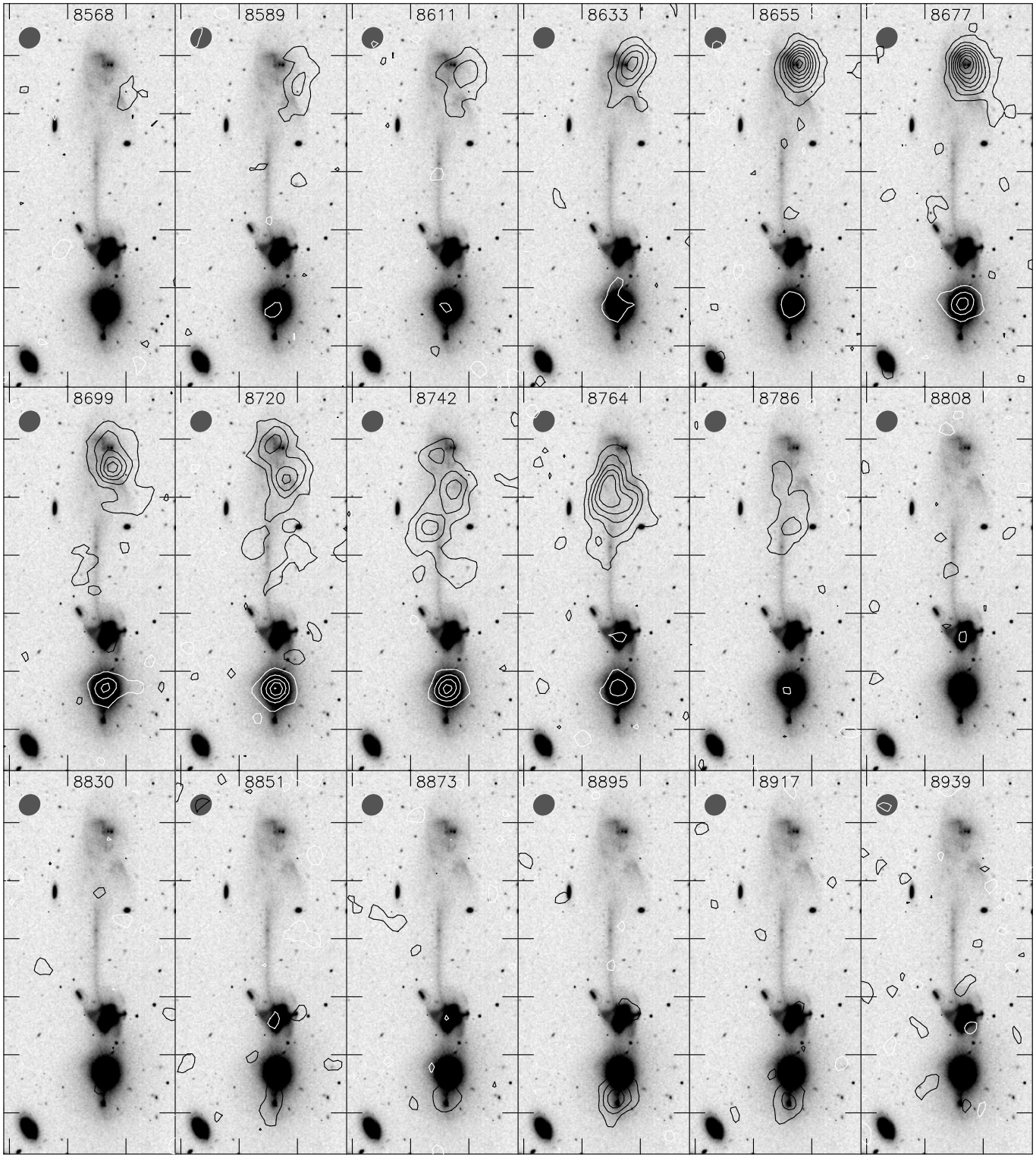

Fig. 3. HI channel maps superimposed on V band images of Arp 105. The velocity, in km s^{-1}, corresponding to each channel is indicated. HI emission is contoured in black and HI absorption in white. The lowest level corresponds to +/- 0.5 mJy $beam^{-1}$, and the interval is 0.7 mJy $beam^{-1}$ for emission contours and 1.1 mJy $beam^{-1}$ for absorption contours. The interval between tickmarks is 1'. The VLA beam size is indicated in the upper left hand corner

Table 4. VLA results

21 cm line emission						Continuum	
Object	$a \times b$ * $''\times''$	a ×b kpc ×kpc	$N_{\rm H}$ cm^{-2}	$M_{\rm HI}$ $M_\odot$	FWHM km s^{-1}	Object	20 cm mJy
(1)	(2)	(3)	(4)	(5)	(6)	(7)	(8)
NGC 3561A - nucleus	-	-	$< 5\times10^{19}$	$< 5\times10^{7}$	-	NGC 3561A	25.8±3
NGC 3561A - Cloud NW	$< 23\times21$	$< 13\times12$	7.5×10^{19}	5×10^{7}	54		
Cloud N3561B	$< 23\times21$	$< 13\times12$	1.4×10^{21}	-	98	NGC 3561B	42.4±3
Cloud A105N	150×70	85×40	9.6×10^{20}	6.6×10^{9}	161		
Cloud A105S	40×35	23×20	3.2×10^{20}	5×10^{8}	70		

* up to a limit of $N_{\rm HI} = 5\times10^{19}$ cm^{-2}

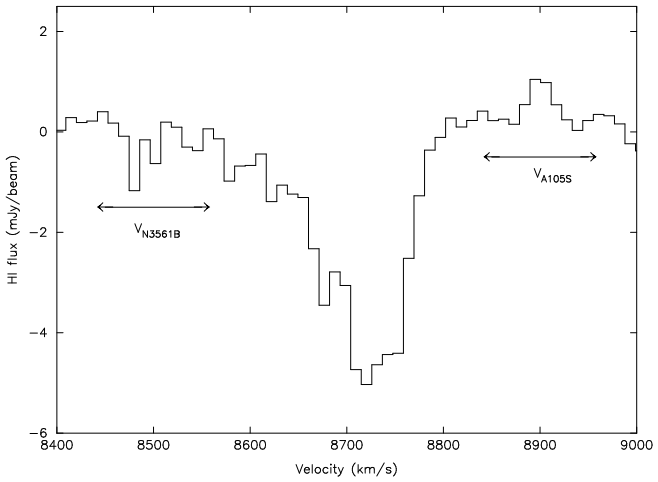

Fig. 4. HI spectrum against the nucleus of NGC 3561B. The optical velocity range of the galaxy ($V_{\rm N3561B}$) and of the blue compact object ($V_{\rm A105S}$) are indicated. The asymmetry of the absorption line suggests accretion of HI by the elliptical galaxy

3.1.3. The southern tail (Clouds N3561B and A105S)

The southern part of Arp 105 shows two distinct systems, one of which is seen in emission, Cloud A105S, and the other in absorption, Cloud N3561B. The former coincides with the blue compact object A105S, the latter with the elliptical galaxy NGC 3561B. Because of the limited spatial resolution of the VLA C+D configuration ($23''\times21''$; 13×12 kpc), and of the small separation between A105S and NGC 3561B ($30''$; 16 kpc), it is only because of their difference in velocity (170 km s^{-1}) that it is possible to differentiate the two.

Cloud A105S is resolved by the VLA beam; it is elongated in the South–North direction, along the thin optical filament that reaches A105S, and located at a distance of 50 kpc from NGC 3561A. It can be traced in emission up to a distance of $5''$, north of the nucleus of NGC 3561B (see Fig. 2), which means that, taking into account the beam size, it extends up to at least $15''$ (8.5 kpc) south of NGC 3561B. The derived mass of Cloud A105S is 5×10^8 $M_\odot$, which is one tenth of the mass of Cloud A105N. The optical and radio velocities towards the nucleus of A105S are comparable; the difference between the two is 30 km s^{-1}. However, although a steep velocity curve in that object had been determined from optical H_α observations (Paper I), the mean velocity of the HI cloud appears to be roughly constant over its total extent (2 beam sizes).

Cloud N3561B is situated in front of the elliptical galaxy NGC 3561B, which is known to host a radio continuum nucleus with a flux density of 42.4 mJy at 20 cm. This radio source, against which HI is seen in absorption, is unresolved at a linear resolution of 180 pc (Batuski et al., 1992). The absorption line spectrum is presented in Fig. 4. The velocity of the peak of the HI absorption is redshifted by 250 km s^{-1} with respect to the velocity of the nucleus, determined from optical longslit spectroscopy (Paper I). Moreover the spectrum appears asymmetric; its blue wing is extending all the way to the optical velocity. A likely interpretation for this is that HI between us and the elliptical galaxy is falling towards it.

In the intermediate region, between the two clouds, the HI spectra show both emission and absorption features (see Fig. 2), at two separate velocities. In between these velocities, there is a "plateau" where no HI is detected. In Sect. 4.2.2, we will discuss the origin of the differences in the velocity distribution and try to determine whether Clouds A105S and N3561B really form a single structure or not.

3.1.4. Other HI detections

Apart from Arp 105, three other HI sources, in the velocity range 8400–9000 km s^{-1}, were detected in the $20'\times20'$ VLA field. Their positions, integrated fluxes and derived velocities, are indicated in Table 5. As we explain in Appendix A, we made additional observations of an object at a velocity around 6250 km s^{-1} which, based on its optical appearance, appeared to be interacting with NGC 3561A (Paper I). In the end, it proved to be unrelated to Arp 105.

3.2. 20 cm radio continuum results

Fig. 5 displays the VLA 20 cm continuum results for a $20'$ field around Arp 105. This map was based on the line–free channels of the combined VLA C– and D–array dataset. The rms noise is about 0.08 mJy. Both the spiral as well as the elliptical are strong continuum sources. Their flux densities are 25.8 ± 0.3

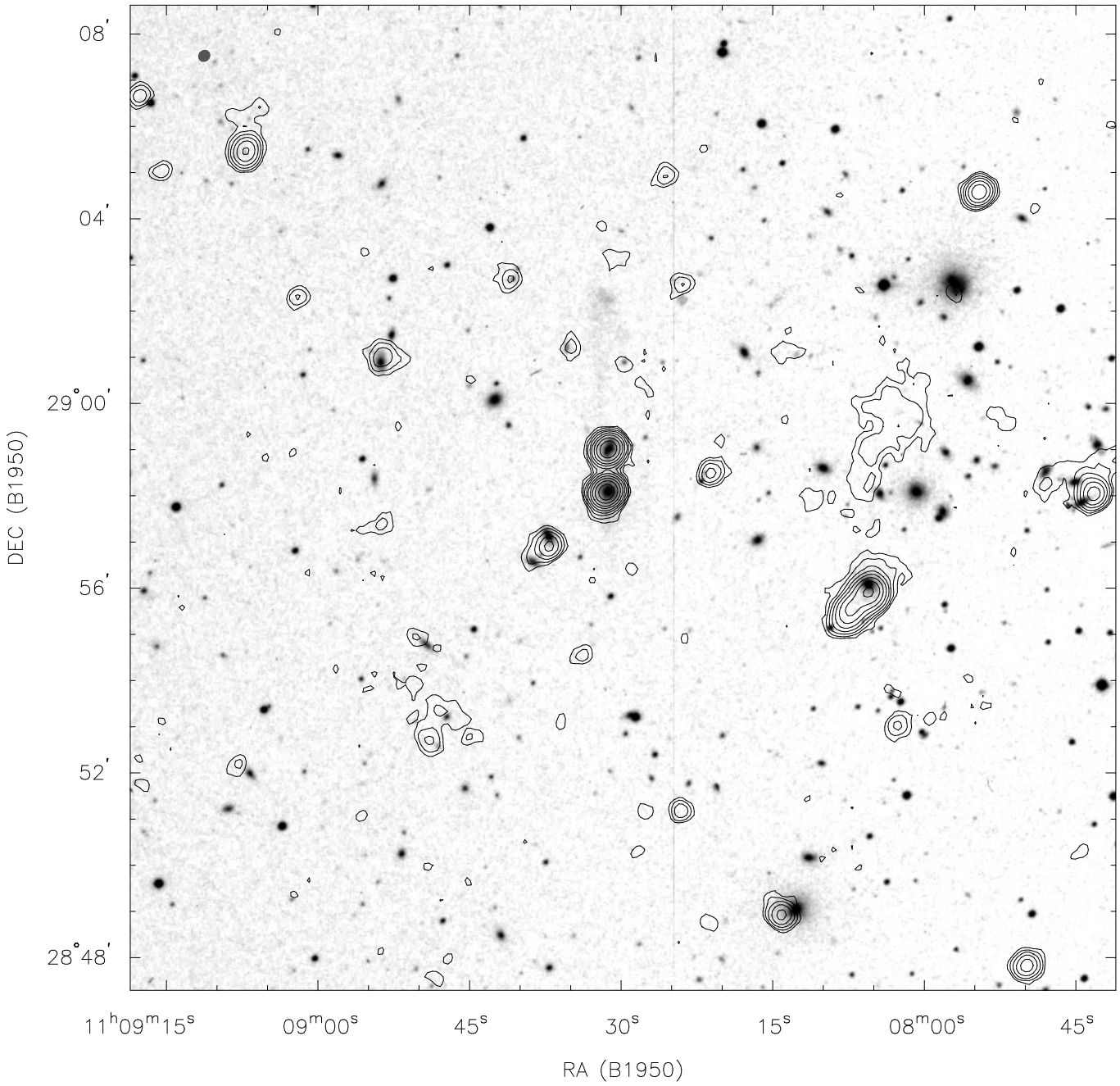

Fig. 5. 20 cm continuum map superimposed on the optical field (a reproduction from the STScI Digital Sky Survey). Radio contours levels are: 0.2, 0.4, 0.6, 1.2, 2.1, 3.9, 7.0, 12.7, 23.0, 41.6 mJy beam^{-1}. The beam size is indicated with a grey disk in the upper left hand corner

and 42.4 $\pm$ 0.3 mJy, respectively. Two extended sources are clearly visible as well, around position α_{1950} = $11^{\rm h}08^{\rm m}05^{\rm s}$; δ_{1950} = 28°59′, near the centre of the cluster Abell 1185, and another one 3′ south of it. The latter one is likely related to the elliptical galaxy NGC 3554 with which it coincides. The northern object, or cloud, is very extended and diffuse with no obvious optical counterpart. It coincides with the X–ray gas as mapped by Beers et al. (1991). Such objects have been seen now in a few clusters of galaxies (see Feretti & Giovannini, 1996, for a review). A follow–up study is in progress.

3.3. The molecular gas

Based on two single dish CO pointings with the IRAM 30–m antenna (Paper I), we already could determine which regions of the system contained molecular gas: no CO was detected within a 20″ diameter region centred on the Magellanic Irregular, A105N. In contrast, a huge amount of molecular gas ($M_{\rm H_2}$ = 10^{10} M$_\odot$, estimated using an N(H$_2$) to I(CO) ratio of 3.6×10^{20} cm^{-2}/K km s^{-1}, and the formula of Sanders et al., 1984) was found in a similar region centred on the spiral. Fig. 1

Table 5. HI detections in the VLA field

α B1950	δ B1950	$M_{\rm HI}$ $M_\odot$	velocity km s^{-1}
$11^h08^m41\overset{s}{.}8$	$28°53'40''$	2.33×10^8	8690
$11^h08^m49\overset{s}{.}1$	$28°54'45''$	3.36×10^8	8610
$11^h08^m53\overset{s}{.}6$	$29°00'50''$	0.95×10^8	8620

Table 6. IRAM Plateau de Bure results

CO(1-0) emission	
NGC 3561A	$\alpha_{\rm B1950} = 11^h08^m31\overset{s}{.}28$
	$\delta_{\rm B1950} = 28°59'00\overset{''}{.}7$
Extension	a × b = 8 ″×10 ″
	a × b = 4.5 kpc × 5.5 kpc
Integrated flux	I(CO) = 11.5 K km s^{-1}
Mass	$M_{\rm H_2} = 10^{10}$ M$_\odot$
2.6 mm continuum	
NGC 3561B	$\alpha_{\rm B1950} = 11^h08^m31\overset{s}{.}45$
	$\delta_{\rm B1950} = 28°58'05\overset{''}{.}4$
Flux	30±3 mJy

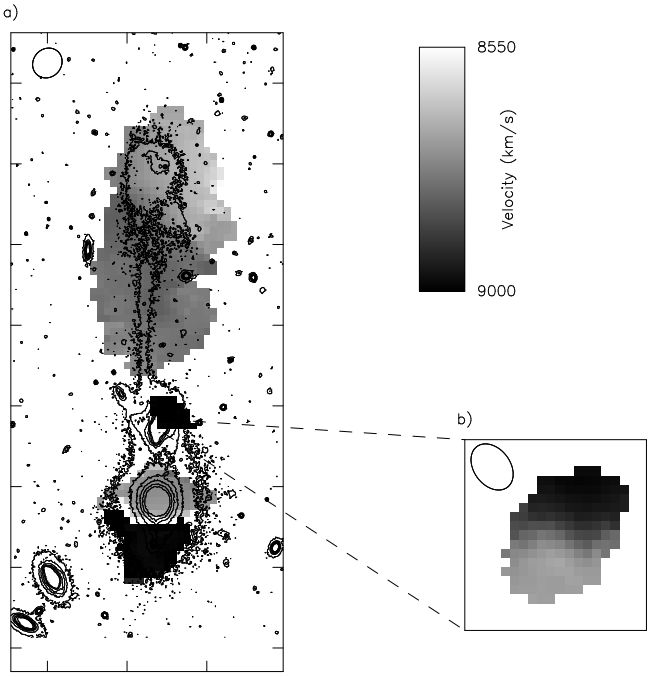

Fig. 6. HI and CO velocity fields. The velocities are coded by grayscale levels, with a scale indicated to the right. They correspond to the peak of the HI emission/absorption lines (Fig. a) and CO emission lines (Fig. b). The VLA and PdB beam sizes are indicated in the upper left corner of each figure. For reference the main optical contours of the system are superimposed. The tickmarks are separated by 1'

shows high resolution follow–up observations with the Plateau de Bure array in the ^{12}CO(1–0) line towards the spiral. Table 6 summarizes the properties of the molecular gas in NGC 3561A.

It is clear from these interferometric observations that the molecular gas, as traced by the CO molecule, is concentrated in the central region of the spiral galaxy. All the emission is found inside a radius of 5″ (2.8 kpc) centred on the nucleus. The CO peak itself lies at less than 0.″7 (0.4 kpc) from the optical nucleus. Given our astrometric precision, which is also 0.″7, there is no evidence for any offset of the CO distribution with respect to the spiral nucleus. Combes et al. (1988) have mapped the molecular gas content of the Virgo galaxy NGC 4438. They showed that, due to the interaction with a companion galaxy, 40% of the gas had been displaced by 1′ (∼ 5 kpc, at the distance of the Virgo cluster). We do not observe such a clear effect in Arp 105. However given the large distance of this system and the sensitivity achieved by the PdB, we would not have detected off–centered clouds less massive than 10^9M$_\odot$ (10% of the total mass). Besides the CO peak emission coincides with the position given by Batuski et al. (1992) for the centre of the centimetric continuum emission to an accuracy of better than 0.″7 (see Table 1).

The total CO flux measured with the Plateau de Bure interferometer matches very well (5% error) that obtained inside the 24″ beam of the 30–m antenna, if one corrects the latter for its beam efficiency. This means that the PdB array has missed no flux.

The distribution of molecular gas in NGC 3561A is particularly smooth and symmetric, apart from a faint East–West extension. The optical image shows, at a larger scale, a similar structure. This faint extension ends to the West in an HII region, and to the East coincides with a diffuse EW feature.

The velocity map (Fig. 6b) of the spiral, derived from the CO(1–0) line observation, shows a barely resolved gradient of 180 km s^{-1} kpc^{-1} inside a nuclear radius of 1″ (0.6 kpc), and a flat rotation curve outside. Fig. 7 presents the velocity curves of NGC 3561A along two position angles: along the South–North direction (PA =0, shown in the main figure), and along a direction closer to the major axis of the galaxy (PA = -35°, shown in the insert in Fig. 7). It combines the HI and CO results from the present paper with the optical velocities derived from H$_\alpha$ longslit spectroscopy (Paper I). All velocities used in this figure are calculated based on the optical Doppler shift definition to allow a direct comparison between the various wavelength ranges. The optical and CO rotation curves of NGC 3561A agree in their overall shape but there are small differences. In particular, on the south–east side, the CO velocities are higher than the optical ones by 70 km s^{-1}. This could be due to the fact that CO and H$_\alpha$ do not have the same optical depth, and therefore do not arise in the same region.

In the direction of the elliptical, we did not detect any CO emission to a limit of 3 Jy km s^{-1}. An unresolved continuum source of 30 mJy is found at the location of the 20 cm radiosource and against which HI is detected in absorption (Table 6).

4. Discussion

The interacting system Arp 105 gathers several noteworthy properties, among others, a complete spatial segregation between its different gas components, a perturbed dynamics of its tidal tails, the accretion of gas by an elliptical galaxy and the formation of dwarf galaxies out of tidal debris. Each of the above mentioned items will be discussed in turn. Also, an atemot will be made to sketch the 3D orientation of the objects involved.

4.1. Origin of the gas segregation in Arp 105

One of the most striking properties of the system Arp 105 is the complete segregation between the HI and CO gas distributions. Huge quantities of HI are found along and at the tip of two tidal tails (6×10^9 $M_\odot$, and 5×10^8 $M_\odot$), while no atomic gas, up to a limit of 5×10^7 $M_\odot$, is detected towards the spiral galaxy. In contrast, massive quantities of molecular gas, 10^{10} $M_\odot$, are found in the core of the spiral and nowhere else.

The close association of the HI clouds with the optical tidal tails, as suspected in Paper I on the basis of single dish observations and confirmed by our VLA data, clearly suggests that the HI depletion in the core of the spiral was tidally induced by interactions. In that respect, Arp 105 is similar to classical colliding and merging galaxies. Hibbard & van Gorkom (1996) have mapped in HI several systems of the Toomre Sequence of colliding galaxies (Toomre, 1977) and have shown that the atomic gas extends along tidal tails from 2 to 7.5 times their standard blue radius, and is deficient in the central regions.

Other characteristics which NGC 3561A has in common with merging galaxies are the high quantities of molecular gas in its core, and the compactness of its distribution (e.g. Young & Scoville, 1991). In the central 1 kpc, we measured a mass surface density of 4.4×10^4 $M_\odot$ pc^{-2}, in the range of that of ultraluminous infrared galaxies (see review by Sanders & Mirabel, 1996). As noted in Paper I, NGC 3561A is luminous in the infrared, and has a far infrared to molecular mass also typical of starburst galaxies. A straightforward explanation for the lack of HI in the inner region and the unusual quantity of H_2 there is that, as a result of shocks following the encounter, the atomic gas dissipates energy, loses angular momentum, and sinks to the central regions where it is transformed into a molecular phase. From numerical simulations, Hibbard (1995) estimates that in the merger NGC 7252, at least half of the initial gas may have been collected in the core of the galaxy.

Besides gravitational forces, other environmental effects, due to the influence of the intergalactic medium, could contribute to the peculiar distribution of the gas in Arp 105. In particular, ram pressure stripping by the intracluster gas (Gunn & Gott, 1972) has been considered to account for HI truncated disks or even anemic disks, observed in cluster spirals (e.g. Cayatte et al., 1994). Although Arp 105 belongs to a rich cluster, the density of the intracluster hot gas at its location, at the edge of the cluster X–ray emission mapped by the Einstein satellite, is too low (Mahdavi et al., 1996), and therefore ram–pressure far too weak, to induce the removal of a cloud as massive as 6×10^9 $M_\odot$ from a spiral galaxy. However, the clear S–N asymmetry of the column density profile, shown by Cloud A105N, could well be due to gas compression at the interface between the moving, tidally expelled, HI cloud and the intergalactic medium. Phookun & Mundy (1995) have argued that ram pressure was responsible for a similar asymmetry, observed in the stripped HI disk of the Virgo galaxy NGC 4654.

Another effect which might play a role is ionization by a background radiation field. This mechanism was originally proposed by Maloney (1992) and Dove & Shull (1994), to account for the sharp decrease of the HI column density in the outskirts of spiral galaxies. Here we would be dealing with a similar, but spatially reversed phenomenon. When moving from the northern tip of the atomic hydrogen cloud coinciding with A105N towards the spiral galaxy, NGC 3561A, the HI surface density declines along the northern tail, to a point where the gas becomes so dilute that it could get ionized by the interstellar radiation field from sources within the spiral galaxy.

Still, in Arp 105, cluster environmental effects have, in comparison with tidal forces, only played a marginal role to shape the overall gas distribution. In Sect. 4.3, we will describe in more detail the interaction taking place in Arp 105, and present our best guess for the relative positions of the objects and their orientations (see sketch, Fig. 9).

4.2. Kinematics of the tidal tails

From the smooth spatial distribution of HI along the tidal tails, it is tempting to argue that all the HI clouds detected in Arp 105 have been expelled from the spiral galaxy, and form a unique structure. In that case, the complex kinematics of the system has to be understood.

4.2.1. The kinematics of the northern tidal tail, A105N

In Sect. 3.1.2, we already pointed out that Cloud A105N is made of several kinematically distinct components. Inspecting the HI data cube along the velocity axis, we can distinguish in the position–velocity (PV–)diagrams (see Fig. 8) at least two systems. One seems associated with the optical tidal tail. Its structure which appears as a partial ellipse in the PV–diagrams is perhaps best visible in the panel labeled 20 at $\alpha = 11^h08^m32\overset{s}{.}287$. The highest (recession) velocities are found mid–way between the spiral and the tip of the tidal arm, with lower velocities on either side. Such a highly curved structure in position–velocity space is a consequence of the interaction, and resembles that observed by Hibbard et al. (1994) in NGC 7252. Hibbard & Mihos (1995) did extensive numerical modeling of the interaction in NGC 7252 and could explain in reasonable detail its structure. They found that energy and angular momentum have a monotonic relationship along the arm which naturally leads to a relationship between radial period and pericentric distance. A curved tail seen edge–on would have a projected velocity field similar to that observed in the first component of the HI tail of Arp 105.

The second component seems to be associated with the dwarf galaxy near the tip of the northern arm. We can identify this system in the position–velocity diagram labeled 24 (taken at $\alpha = 11^h08^m30\overset{s}{.}762$). This feature is oriented almost exactly North–South, which implies that we are seeing this subsystem almost edge–on. It seems to be extending from $\delta = 29°02'20''$ and a velocity of 8640 km s^{-1} to $\delta = 29°01'10''$ and a velocity of 8770 km s^{-1}. The PV–map would therefore suggest the presence within the tidal tail of a kinematically decoupled cloud, having a gradient of about 130 km s^{-1} over a distance of 40 kpc. If we assume that we are dealing with (solid body) rotation, we derive a dynamical mass of $M_{dyn} = \frac{V^2 R}{G}$ of 2.4×10^{10} M$_\odot$. Most of the HI would belong to this feature and, corrected for He and heavier elements, the gas mass associated would account for about 25% of the dynamical mass.

All the above calculations were made assuming that we could separate perfectly both HI components which, given the limited VLA resolution, both spatially and in velocity, is clearly not the case. The spatial extent, and velocity gradient of the independent feature, are therefore rather uncertain. The dynamical mass, derived above, should be considered as an upper limit only. It supersedes the one quoted in Paper I, estimated from single–dish observations.

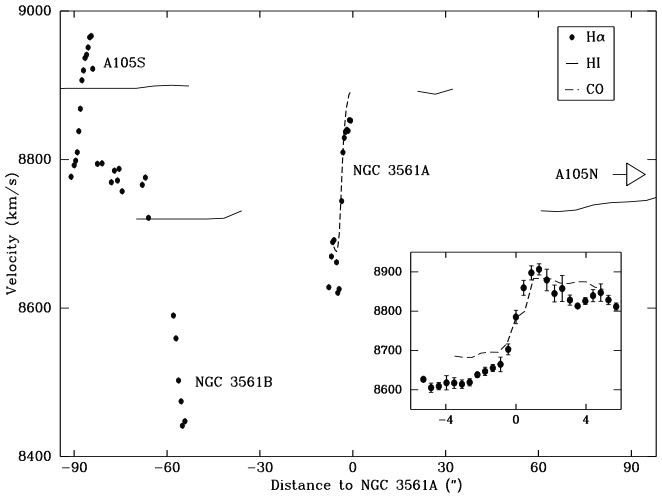

Fig. 7. South–North velocity profile of the southern region of Arp 105. Data from Hα, HI and CO observations have been compiled. A105N is situated to the right, outside the figure. In the insert is shown the rotation curve of the spiral galaxy along PA=-35°. The units are the same as in the main figure. All velocities are calculated based on the optical Doppler shift definition and are heliocentric

4.2.2. The kinematics of the southern tidal tail, A105S

Fig. 7 gathers all the multiwavelength information available regarding the velocity distribution of the southern region of Arp 105, along a South–North axis, encompassing A105S, the optical filament, the elliptical galaxy, the spiral galaxy, and the beginning of the northern tidal tail. Plain dots represent the velocity measurements of the ionized gas, determined from optical longslit spectroscopy. Plain lines represent the HI velocity profile, along the S–N axis, for both emitting and absorbing components. Finally the CO velocity curve along the S–N axis is shown with a dashed line. Table 7 gives for each component the velocity measured on their optical nuclei and, in parentheses, the total velocity range, for the Hα, HI and CO observations.

The velocity field of the southern region is strikingly complex. Cloud N3561B seen in absorption in front of the elliptical, and Cloud A105S seen in emission, coinciding with A105S, have mean velocities which differ by 170 km s^{-1}. The optical velocity of NGC 3561B, in turn, is lower by 250 km s^{-1} than that of Cloud N3561B. The ionized gas in the blue compact galaxy, A105S, features a strong velocity gradient.

All these features raise the question whether the different clouds observed along the tidal tails of Arp 105, especially in the southern one, belong to the same overall HI distribution, are overlapping each other, or are kinematically and spatially distinct.

— Hypothesis 1: A105S and N3561B are two independent clouds

In the following, we assume that Clouds A105S and N3561B are independent, having different mean velocities (resp. 8890 km s^{-1} and 8720 km s^{-1}). Both clouds might spatially overlap along the line of sight towards NGC 3561B. Cloud A105S is seen in emission along the southern tail up to the nucleus of the elliptical, where a faint emission feature can still be seen (see Fig. 4). Its weakness could result from a low intrinsic HI column density there and/or contamination by absorption. Extrapolating the HI column density profile of Cloud A105S, assuming that like in Cloud A105N, the flux declines linearly along the tail when approaching the spiral, and taking into account the fact that no HI is seen in emission north of the radiosource, we get at the position of the radiosource an upper limit of 2 mJy beam^{-1}. The faint emission feature is only 1 mJy beam^{-1} which suggests that it might be attenuated by absorption against the bright nucleus of the elliptical. In that case one can in principle determine the spin temperature, $T_{\rm S}$, of the gas, using the method described by Dickey et al. (1992). $T_{\rm S}$ is given by:

$$T_{\rm S} = \frac{S_{\rm em}}{0.82(1-\exp(-\tau))} \quad (1)$$

where τ, the optical depth, can be determined from the formula:

$$\exp(-\tau) = 1 + \frac{S_{\rm abs} - S_{\rm em}}{S_{\rm c}} \quad (2)$$

In these equations, $S_{\rm c}$, is the continuum flux, $S_{\rm abs}$, the line flux measured on the radiosource, affected by the absorption (+1 mJy beam^{-1}), and $S_{\rm em}$, the line flux that would have been measured at the position of the radiosource if there were no absorption (+2 mJy beam^{-1}). The factor 0.82 results from the gain of the telescope and depends on the array configuration (and thus beam size). With the known flux density of the continuum

Table 7. Velocity field

Object	H_α	HI km s^{-1}	CO
Northern tail – A105N	8670	8670 (8620–8780)	–
NGC 3561A – nucleus	8810 (8600–8900)	–	8780 (8670–8890)
NGC 3561A – cloud NW	–	8900	–
NGC 3561B – nucleus	8500 (8450–8590)	8720 (8670–8750)	–
Southern tail – HII knots	8780 (8760–8820)		–
Southern tail – A105S	8920 (8780–8960)	8890 (8850–8920)	–
Intruder	6080	6250 (6200–6300)	–

source of 42.4 mJy we derive an optical depth less than 0.02, and a spin temperature higher than 100 K.

Cloud N3561B is only seen in absorption. No HI in emission outside the radiosource was detected at the velocity of the absorption line, up to a limit of 0.5 mJy beam^{-1}. This means that either the HI column density of cloud N3561B drops sharply outside the radiosource, or that the gas temperature is extremely low, so that the HI cannot be seen in emission. Given our sensitivity, the lowest column density measurable in emission at 2.5 σ is 5×10^{19} cm^{-2}. $N_{\rm HI}$ is given by:

$$N_{\rm HI} = 1.823\times10^{18} T_{\rm s} \tau \Delta(V) ({\rm cm}^{-2}) \quad (3)$$

Assuming $S_{\rm abs} >> S_{\rm em}$, we derive τ = 0.15 at the absorption peak. Since $\Delta(V)$ will be greater or equal than 10 km s^{-1}, our VLA velocity resolution, one obtains, from Eq. 3, an upper limit for the spin temperature of 20 K.

In the above calculations, it was assumed that the two HI clouds were extended enough — Cloud A105S in the direction of the elliptical, and Cloud N3561B outside of it — so that the determination of spin temperatures is relevant. If that hypothesis is correct, it implies that both clouds have rather different physical properties and origins: they could have been expelled from several regions of the spiral, during different passages of the elliptical; the latter galaxy could also have accreted HI gas from other cluster galaxies.

— Hypothesis 2: N3561B and A105S form a single cloud

We now make the hypothesis that N3561B and A105S form a single HI cloud, corresponding to the counter tidal tail of NGC 3561A. We can estimate the spin temperature, under the simple, naive assumption that it remains constant all along the tidal tail. Like in hypothesis 1, we take for the interpolated emission flux, an upper limit of $S_{\rm em}$ = 2 mJy beam^{-1}. The absorption flux at its peak is $S_{\rm abs} = -5$ mJy beam^{-1}. From Eq. 2, we derive τ = 0.17, and from Eq. 1, $T_{\rm s} < 14$ K.

The different velocities measured for Clouds N3561B and A105S imply that the HI tail is pulled strongly towards the elliptical. Taking into account the VLA beam size, and the fact that the HI in emission, at the velocity of A105S, is seen up to 5″ north of the radiosource, the velocity gradient should be of order 170 km s^{-1} over less than 5″. Even if this drop along the tail is not directly visible because of the limited spatial resolution, it should appear in the HI spectrum as an asymmetry towards the higher velocities, in addition to a similar wing seen towards the blue. This is definitely not seen (see Fig. 4).

An alternative interpretation for the velocity field presented in Fig. 7 is that the southern HI tail might have a roughly constant mean radial velocity, equal to that measured for Cloud N3561B, $V_{\rm N3561B} \sim 8720$ km s^{-1}. An argument in favor of that hypothesis is that the optical HII knots seen along the southern tail north of A105S as well as the very tip of the filament, have velocities that differ from $V_{\rm N3561B}$ by less than 50 km s^{-1}, and therefore might be associated with a single HI tail. Only the gas near the elliptical, which seems to accrete part of it (see Sect. 4.4), and in the very core of A105S might have a discrepant behaviour. The velocity determined for Cloud A105S, 170 km s^{-1} higher than $V_{\rm N3561B}$, is coincident with the centre of the rotation curve measured in H_α on the dwarf galaxy. Due to the large VLA beam size, direct evidence for rotation of the atomic hydrogen cannot be provided. However the HI spectra show "blue" wings that are indicative of a global motion of the gas (see Fig 2). Hence our velocity data might support the idea that HI along the southern tail has been gravitationally pulled away, to form the blue compact galaxy A105S. The latter object would then have already gained its kinematic independence.

Obviously the lack of spatial resolution for the HI observations make it difficult to give a definitive answer to the issue whether the HI clouds seen south of NGC 3561A belong to the same tidal tail, were ejected from different regions of the spiral, or have different origins, although the interaction has undoubtly played a crucial role in their formation. Unfortunately, VLA configurations which provide better spatial resolution require to get a high enough signal–to–noise ratio much higher fluxes than those seen in Arp 105.

4.3. A 3D view of the interaction

From the shape and the kinematics of the tidal tails, it is possible to build a rough overall picture of the interaction.

One should note first that we are dealing here with a fundamentally different situation than discussed most often in the literature, namely the encounter between an elliptical and a spiral galaxy, rather than an interaction between two spirals. In the latter situation, two giant tails spread out, one from each disk.

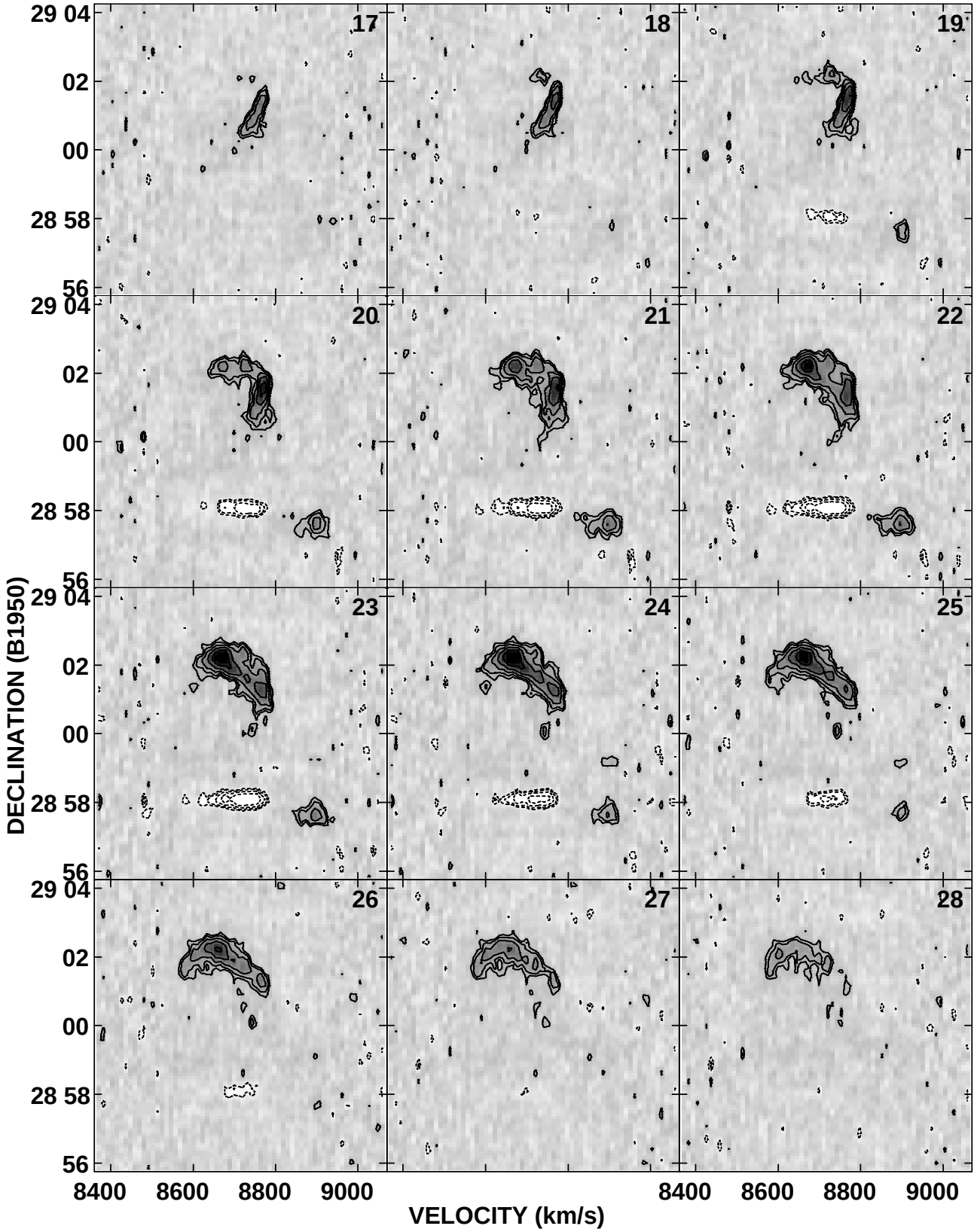

Fig. 8. Series of HI position–velocity maps taken along the North–South direction through the Arp 105 system. The x–axis is velocity, the y–axis declination. The number listed in the top right hand corner of each panel can be used to recover the right ascension: panel 26 corresponds to a cross cut at $11^h08^m30^s$ whereas lower numbered panels were made along lines shifted by $n \times 5''$ or $n \times 0.^s38$ to the East. Contour levels are drawn at -2.5, -1.5, -0.9, -0.6, 0.6, 0.9, 1.5, 2.5, 4.0, and 4.0 mJy beam^{-1}

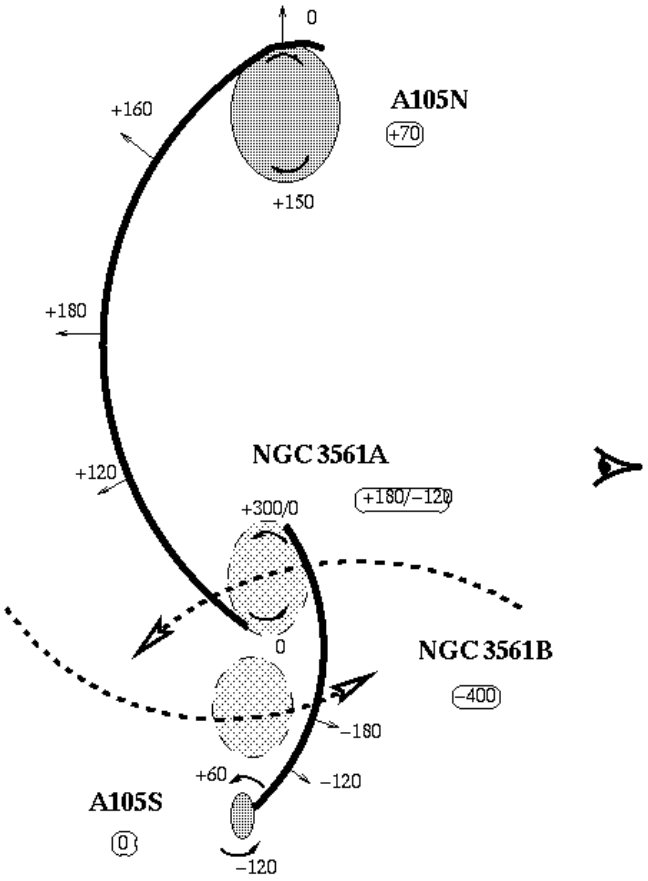

Fig. 9. Possible sketch for the 3D geometry of the encounter. The system is displayed as it would be observed if looking perpendicular to the plane of the interaction. The observer sees the system close to "edge–on", i.e., within the plane of the interaction. The VLA and Hα radial velocities are indicated. For the northern resp. southern tail, the velocity reference is that of the lower resp. upper end of the spiral velocity curve (8600 km s^{-1}and 8900 km s^{-1})

Shorter counter–tails form on the opposite side of each galaxy, and then rapidly collide and merge (e.g., Barnes, 1988; Hibbard, 1995; Mihos & Hernquist, 1996). In a spiral–elliptical collision, only one long tail and a short counter–tail form from the spiral (Elmegreen et al., 1993). Going into more detail, numerical models of such collisions are characterized by the sparseness of material between the spiral and the elliptical, and the accumulation of tidally expelled material in the vicinity of the elliptical. A good example for this is presented by Barnes & Hernquist (1992) who, in their Fig. 3, show the fate of one disk as it is perturbed by its partner, which is approximated by a point–mass. The similarities between this case and Arp 105 are remarkable. In the latter system, the northern arm is the main tidal feature; a very diffuse optical counter–tail is seen between NGC 3561A and NGC 3561B (Paper I), and HI clouds have gathered south of NGC 3561B.

From the comparison of the straight curve of the northern arm, with the highly curved tails produced by numerical models, one can conclude that the interaction taking place is seen almost edge–on (i.e., the observer is located close to the plane of the interaction). This is confirmed, as shown in the previous Sect. 4.2.1, by the kinematics of the northern tail.

We must be past perigalacticon, but still within the first passage. The tidal arm is still developing and most material (gas and stars) is moving outward and has not started to fall back towards the spiral. Relative to the observer, the elliptical is coming from behind the spiral and is now moving towards the observer; the spiral is moving away with respect to centre of gravity of the system. The tidal arm is still moving mostly away from the spiral, no gas having reached its maximum separation from the spiral yet. The elliptical is likely embedded within the counter–tail. A possible sketch for the interaction is presented in Fig. 9. In this figure, the kinematically decoupled components seen in the gas clouds have been represented, and their sense of rotation indicated. A105N is counterrotating with respect to NGC 3561A; A105S had the same sense of rotation as the spiral.

Without a more thorough analysis including numerical simulations, it will be difficult to define more precisely the true three dimensional shape and the motions of the gas in the tails. Arp 105 should be an excellent case for numerical modeling as it is in in an early stage of an interaction between a spiral and an elliptical, an encounter which results in only one major tidal arm, thus avoiding the chaos normally seen in disk–disk collisions.

4.4. Gas accretion towards the elliptical galaxy

The HI absorption spectrum towards NGC 3561B discloses the presence of atomic hydrogen in front of the elliptical. The shape of the line — a blue wing towards the systemic velocity of the galaxy — suggests inflow towards the nucleus. In addition, indirect signs of former accretion by the elliptical are seen. The optical image exhibits dust lanes (see Fig. 3 in Paper I) and ionized gas was found in the core of the galaxy, which is classified as a LINER from optical spectroscopy. Our interpretation is that part of the HI may feed a central engine.

The mass of the absorption cloud associated with NGC 3561B may be estimated from the following formula:

$$M_{\rm HI} = \pi R^2 m_{\rm H} N_{\rm HI} \tag{4}$$

R is the cloud size; the column density is given by

$$N_{\rm HI} = 1.823\times10^{18} T_{\rm S} \int \tau dV \tag{5}$$

Finally taking values characteristic of Cloud N3561B, one obtains:

$$\frac{M_{\rm HI}}{\rm M_\odot} = 2\times10^9 \left(\frac{R}{5.3\ \rm kpc}\right)\left(\frac{T_{\rm S}}{100\ \rm K}\right) \tag{6}$$

For a typical age for the formation of the system of 1 Gyr and taking reasonable values of $T_{\rm S}$ between 10 K and 100 K, the accretion rate would be of the order of 0.2–2 M$_\odot$yr^{-1}. Clouds of atomic hydrogen associated with early type galaxies, ellipticals or lenticulars, are now routinely detected. From

a sample 26 ellipticals, Huchtmeier (1994) has derived a mean HI mass to blue luminosity, equal to 0.01, to be compared to $0.1(\frac{T_S}{100\,K})$ $M_\odot/L_\odot$, for NGC 3561B.

It is commonly believed that the atomic gas detected in early type galaxies has an external origin: for instance, gas rich dwarf galaxies which are swallowed up or HI clouds torn away from another galaxy (Knapp et al., 1985; Wardle & Knapp, 1986), although most of the time all traces of the suppliers of this gas have disappeared. As discussed in the previous Sect. 4.2.4, it is likely that the HI detected towards NGC 3561B, was tidally pulled out from its companion, NGC 3561A. Arp 105 could therefore provide direct evidence of a transfer of gas between a spiral and an elliptical galaxy.

4.5. Properties of the tidal dwarf galaxies

Recently an exciting result has emerged from various studies of the environment of interacting systems: the discovery of a particular class of dwarf galaxies: the tidal dwarfs, formed out of material pulled out from colliding galaxies. These recycled objects, often found at more than 100 kpc from their parent galaxies, are currently undergoing vigorous star forming episodes (Schweizer, 1978, Mirabel et al., 1992, Yoshida et al., 1994, Duc, 1995). They are also characterized by a rather high metallicity for their mass (Duc, 1995).

With arguments based upon the optical morphology of Arp 105, we pointed out in Paper I that the two small galaxies A105N and A105S were likely to have a tidal origin. Our VLA observations presented here stress this even more. First, the overall structure of the HI tails is remarkably similar to the distribution of the tidal material observed in classical interacting objects, in agreement with numerical models of spiral–galaxy encounters. If, on the contrary, A105N and S existed before the interaction between NGC 3561A/B, both hosting high quantities of HI, how could such low–mass objects have been able to hang on to it, whereas a massive spiral, like NGC 3561A, has almost completely lost its gas?

The HI and CO data reported here allow for a better characterization of the gaseous properties of tidal dwarfs. With an HI mass to blue luminosity ratio of 1.3 and 0.5 $M_\odot/L_\odot$, A105N and A105S may be classified as gas rich. The young tidal dwarf galaxies have not yet exhausted their gas supplies, and are currently forming their first generation of stars (excluding their old star population, pulled out from the parent galaxies). Since active star formation is taking place, one would expect molecular gas to be abundant as well. We did not detect with the IRAM 30–m single dish antenna (see Paper I) any CO in A105N. Other studies (e.g. Smith & Higdon, 1994) also failed at finding molecular gas in tidal tails. Obviously due to the poorly known conversion coefficient between the H_2 column density and the CO flux in galaxies other than the Milky Way, any conclusion regarding the real absence of molecular gas in tidal dwarfs is premature. Classical dIrr galaxies seem also to be deficient in CO gas (e.g. Gallagher & Hunter, 1984, Israel et al., 1995). One explanation for this deficiency is their low metallicity, and therefore low content of CO. In the case of tidal galaxies, this argument is less relevant. Due to their very nature, "recycled objects" cannot be metal poor (Duc, 1995).

The HI gas clouds of Arp 105 have high velocity dispersions; the mean σ is 26 km s^{-1} for A105N, and 20 km s^{-1} for A105S. In A105N the velocity dispersion reaches much higher values in some places, but as emphasized before, this is due to line blending of a multiple system. For comparison a typical value of σ in isolated spiral galaxies is less than 10 km s^{-1}. High velocity dispersions in tidal tails are actually predicted in a numerical model of tidal dwarf formation proposed by Elmegreen et al. (1993). Following the Jeans criterion, high mass clouds, of $\sim 10^8$ $M_\odot$, can only be formed if they have σ of the order of 20–30 km s^{-1}. The asymmetry of the HI column density profile of Cloud A105N (Sect. 4.1) suggests that pressure exerted by the intra–cluster medium (ICM) may play a role in the collapse of these tidally expelled clouds. It might be useful to carry out X–ray observations in order to confirm the presence of shocks at the interface between the HI and the ICM.

Our VLA and H_α observations are consistent with the idea that the two tidal dwarfs A105N and A105S are already kinematically independent objects. They provide for the first time evidence that some tidal objects might be self–gravitating, and therefore be "true" galaxies. A105N/S show possible signs of rotation, that have to be confirmed. In Sect. 4.2.1, we have derived an upper limit for the dynamical mass of A105N of 2.4×10^{10} $M_\odot$. According to Paper I, the blue luminosity is 4.7×10^9 $L_\odot$. Therefore if A105N is indeed self–gravitating, its M/L_B ratio would be less than 5. In A105S, the lack of spatial resolution makes any mass determination based on HI data unreliable. However using the rotation curve determined in that object from H_α observations, we estimated in Paper I a dynamical mass of $10^9 M_\odot$, and an M/L_B ratio of the order of 1. These mass to luminosity ratio are indicative of a low dark matter content, in agreement with the predictions of numerical models by Barnes & Hernquist (1992).

5. Conclusion

Using interferometric HI and CO observations, we found an extreme spatial segregation between the atomic and molecular gas in Arp 105 (NGC 3561A/B). These gas distributions are consistent with the idea that, as result of a collision, one fraction of the atomic gas of NGC 3561A has been tidally pulled out into the intergalactic medium, supplying, for one part, tidal dwarf galaxies, and for the other, the active nucleus of NGC 3561B, whereas another fraction has sunken towards its central region, where it was transformed into molecular gas. In that respect, Arp 105 exhibits all the phenomena previously observed in typical mergers, although it is a far less evolved interacting system.

Our multi–wavelength study reveals a complex dynamics. In the central region of the spiral, the molecular and ionized gas show flat rotation curves. In the southern part of the system, the HI clouds associated with NGC 3561B and A105S have discrepant velocities, which suggests that either they have different origins, or that they used to belong to one structure, part of which has collapsed and has formed the tidal dwarf A105S.

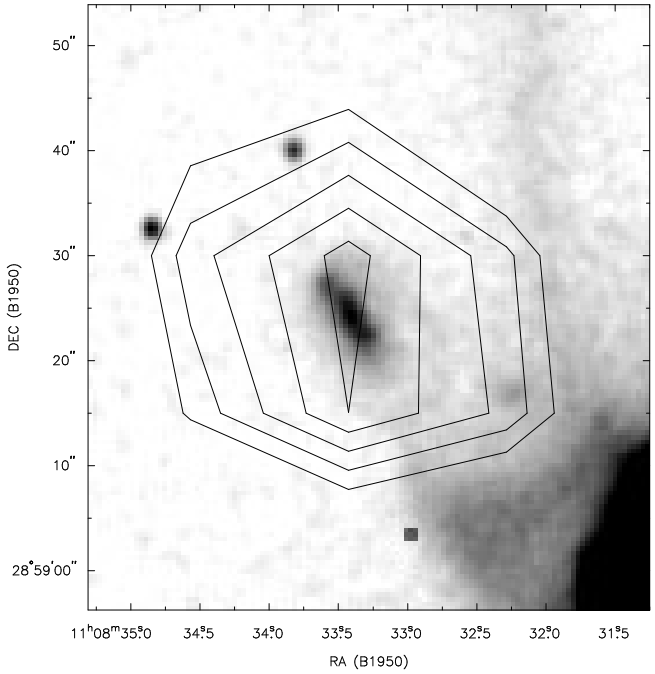

Fig. 10. VLA D–configuration map of the HI in the intruder galaxy East of NGC 3561A. The contours (11.0, 11.7, 12.5, 13.2, 14.0 $\times 10^{19}$ cm^{-2}) are superimposed on an optical image

A similar phenomenon might have occurred in the northern HI clouds, where we observe, within the HI tail, a kinematically decoupled component, associated with the star forming dwarf A105N. Both tidal objects show possible signs of rotation.

The observations reported here provide for the first time indications that some tidal dwarfs might already be gravitationally bound and are therefore likely to become independent galaxies.

Acknowledgements. We thank our anonymous referee for useful comments. EB is grateful to the Service d'Astrophysique at Saclay for inviting him for a month during which most of the VLA data reduction was performed. PAD thanks the Departemento de Astronomía of the Instituto de Física of the Universidad de Guanajuato (México), for its hospitality, which greatly helped to getting this paper finished.

Appendix A. The intruder galaxy

In Paper I, we proposed the hypothesis that the small galaxy, near the Eastern arm of the spiral galaxy, could be a companion flying by at a high relative velocity (ΔV = 2700 km s^{-1}). The main arguments were the apparent optical connection between both objects and a measured difference between the systemic velocity as obtained from the single dish Arecibo observations in HI, and the optical value. That difference could have resulted from a gravitational interaction. To test that idea a second set of observations was obtained, but in the D–array only, of the same field and at a redshift of 6250 km s^{-1}, i.e., centred on the recession velocity of the potentially interacting galaxy. The set–up was very similar to that of the observations described above, except that we used the conventional arrangement in which both R and L polarizations cover the same frequency range; in this case 64 channels at 48.8 kHz (10.9 km s^{-1}). Some 1^h15^m was obtained on 8 November 1993 and an additional 2^h10^m on 18 January 1994. The same calibrators were used as for our main observations. Also, we used the same method to eliminate the effects of solar interference. The two days worth of data were merged in the *uv*–plane and Fourier transformed.

The resulting HI column density map is presented in Fig. 10, superimposed on an optical image. It is clear that the HI peak coincides exactly with the nucleus of the galaxy. Had it suffered a tidal interaction, there would have likely been a spatial shift or signs of an asymmetry. Therefore, we conclude that this object is most probably a foreground galaxy, perhaps belonging to the cluster. Note that Beers et al. (1991) have shown that Abell 1185 contains a group of galaxies with velocities around 6000 km s^{-1} of which this object might be a member.

References

Arp, H.: 1966, Atlas of Peculiar Galaxies, California Institute of Technology, Pasadena
Arp, H. & Madore, B.: 1987, A catalog of Southern Peculiar Galaxies and Associations, Cambridge University, Cambridge
Baars, J. W. M., Genzel, R., Pauliny-Toth, I. I. K., & Witzel, A.: 1977, A&A 61, 99
Barnes, J. E.: 1988, ApJ 331, 699
Barnes, J. E. & Hernquist, L.: 1992, Nature 360, 715
Batuski, D. J., Hanisch, R. J., & Burns, J. O.: 1992, AJ 103, 1077
Beers, T. C., Forman, W., Huchra, J. P., Jones, C., & Gebhard, K.: 1991, AJ 102, 158
Cayatte, V., Kotanyi, C., Balkowski, C., & van Gorkom, J. H.: 1994, AJ 107, 1003
Combes, F., Dupraz, C., Casoli, F., & Pagani, L.: 1988, A&A 203, 9
Dickey, J. M., Brinks, E., & Puche, D.: 1992, ApJ 385, 501
Dove, J. B. & Shull, J. M.: 1994, ApJ 423, 196
Duc, P.-A.: 1995, Ph.D. thesis, Universite Paris VI
Duc, P.-A. & Mirabel, I. F.: 1994, A&A 289, 83
Elmegreen, B. G., Kaufman, M., & Thomasson, M.: 1993, ApJ 412, 90
Feretti, L. & Giovannini, G.: 1996, in I. S. 175 (ed.), Extragalactic Radio Sources, p. 333, Kluwer
Gallagher, J. & Hunter, D.: 1984, Ann. Rev. Astron. Astrophys. 22, 37
Giovanelli, R. & Haynes, M. P.: 1988, in G. L. Verschuur & K. I. Kellermann (eds.), Galactic and Extra-galactic Radio Astronomy, p. 522, Springer-Verlag
Guilloteau, S., Delannoy, J., Downes, D., Greve, A., Guélin, M., Lucas, R., Morris, D., Radford, S. J. E., Wink, J., & Cernicharo, J.: 1992, A&A 262, 624
Gunn, J. E. & Gott, J. R.: 1972, ApJ 176, 1
Hibbard, J. E.: 1995, Ph.D. thesis, Columbia University
Hibbard, J. E., Guhathakurta, P., van Gorkom, J. H., & Schweizer, F.: 1994, AJ 107, 67
Hibbard, J. E. & Mihos, J. C.: 1995, AJ 110, 140
Hibbard, J. E. & van Gorkom, J. H.: 1996, AJ 111, 655
Huchtmeier, W. K.: 1994, A&A 286, 389
Israel, F. P., Tacconi, L. J., & Baas, F.: 1995, A&A 295, 599
Knapp, G. R., Turner, E. L., & Cunniffe, P. E.: 1985, AJ 90, 454

Mahdavi, A., Geller, M. J., Fabricant, D. G., Kurtz, M. J., Postman, M., & Mclean, B.: 1996, AJ 111, 64
Maloney, P.: 1992, ApJ 398, L89
Mihos, J. C. & Hernquist, L.: 1996, ApJ 464, 641
Mirabel, I. F., Dottori, H., & Lutz, D.: 1992, A&A 256, L19
Napier, P. J., Thompson, A. R., & Ekers, R. D.: 1983, IEEEP 71, 1295
Phookun, B. & Mundy, L. G.: 1995, ApJ 453, 154
Sanders, D. B. & Mirabel, I. F.: 1996, ARA&A 34, 749
Sanders, D. B., Solomon, P. M., & Scoville, N. Z.: 1984, ApJ 276, 182
Sargent, A. & Scoville, N.: 1991, ApJ 366, 1
Schweizer, F.: 1978, in E. Berkhuijsen & R. Wielebinski (eds.), Structure and Properties of Nearby Galaxies, p. 279, Dordrecht, D. Reidel Publishing Co.
Scoville, N. Z., Sargent, A. I., Sanders, D. B., & Soifer, B. T.: 1991, ApJ 366, L5
Smith, B. J. & Higdon, J. L.: 1994, AJ preprint
Toomre, A.: 1977, in B. M. Tinsley & R. B. Larson (eds.), The Evolution of Galaxies and Stellar Populations, p. 401, New Haven: Yale University Observatory
Toomre, A. & Toomre, J.: 1972, ApJ 178, 623
van der Hulst, J. M.: 1979, A&A 71, 131
Veron, M. P., Veron, P., Adgie, R. L., & Gent, H.: 1976, A&A 47, 401
Vorontsov-Velyaminov, B.: 1959, Atlas and Catalogue of Interacting Galaxies, Sternberg Institute, Moscow State University, Moscow
Wardle, M. & Knapp, G. R.: 1986, AJ 91, 23
Yoshida, M., Taniguchi, Y., & Murayama, T.: 1994, PASJ 46, L195
Young, I. S. & Scoville, N. Z.: 1991, ARA&A 29, 581

This article was processed by the author using Springer-Verlag LaTeX A&A style file *L-AA* version 3.